Experimental observations of bubble response and light intensity near the threshold for single bubble sonoluminescence in an air-water system

D. Felipe Gaitan
National Center for Physical Acoustics, University of Mississippi, University, Mississippi 38677

R. Glynn Holt
Department of Aerospace and Mechanical Engineering, Boston University, Boston, Massachusetts 02215

(Received 2 June 1998)

Single bubble sonoluminescence in an air-water system has been shown to occur along a unique surface in the acoustic pressure-ambient radius-gas concentration parameter space where the bubble is stable both in shape and in (average) size. In this paper, we show how the bubble deviates from the expected path (traced by the shape-instability threshold as a function of pressure) in order to reach the observed stability. We also present measurements of the expansion ratio ($R_{\max}/R_0$) for bubbles near the threshold for light emission. The results suggest that maximal bubble radial response is an insufficient criterion for the onset of light emission, and we present data for the dependence of the emitted light on several parameters. [S1063-651X(99)07905-2]

PACS number(s): 47.55.Dz, 43.25.+y, 43.35.+d, 78.60.Mq

INTRODUCTION

Single bubble sonoluminescence (SBSL) is a phenomenon in which an acoustically levitated bubble is made to oscillate so violently that pulses of light are emitted at the time of collapse [1]. In contrast to the previously known phenomenon now called multibubble sonoluminescence (MBSL), SBSL involves only a single bubble that becomes stabilized against shape instabilities (SI) and (bubble size) growth [2]. The typical mechanisms responsible for SI are the Faraday and the Rayleigh-Taylor instabilities [3], and for growth, rectified diffusion (RD) [4]. Thus, for SBSL to be possible, three conditions must be met: (i) the bubble must be below the SI threshold; (ii) for zero net growth, the bubble must be at the RD threshold; and (iii) for a stable equilibrium, the RD threshold must be such that a small decrease (increase) in the bubble size places the bubble in a growth (dissolution) region. This occurs when the slope of the RD threshold curve is positive when plotted as $P_{\text{threshold}}$ versus R_0. In this paper we show how the bubble deviates from the expected path in the acoustic pressure-ambient radius (P_a, R_0) [5] parameter space in order to achieve the observed stability [6]. The cause of the deviation, according to the hypothesis of Lohse *et al.* [7], is the onset of internal chemical reactions occurring during the bubble collapse, which results in a much lower growth rate by RD since the reacting species (dissociated N_2 and O_2 primarily) no longer participate in the cycle-averaged mass exchange

APPARATUS

Measurements were made using an apparatus and techniques first reported in [2]. The apparatus is shown here in Fig. 1 and consisted of a cylindrical levitation cell (see Gaitan *et al.* in Ref. [1]) made up of two hollow, piezoelectric PZT ceramics. The cell was filled to the top and sealed with a quartz disk 3.2 mm ($\frac{1}{8}$ in.) thick in order to keep the dissolved gas concentration constant. Two barbed hose connectors, which served as an inlet and an outlet, were attached to the quartz disk. A 2-mm-diam hydrophone was positioned near the bubble in order to monitor the driving acoustic pressure P_a. The hydrophone was calibrated using a modification of the levitation technique described in Gaitan *et al.* (Ref. [1]). The most important aspect of the modification was the inclusion of the measured spatial pressure gradient (which can vary for different levitation cells) in the description of the acoustic force. A 7 mW He-Ne laser and a Hamamatsu H5783-00 photomultiplier tube were used to monitor the dynamic bubble radius using the Mie scattering technique developed by Hansen and Holt [8] for single acoustically levitated bubbles. Images of the bubble were obtained using a Cohu 4910 CCD camera, a Questar QM100 long-distance microscope, and a pulsed, frequency-doubled YAG laser to back-illuminate the bubble. The ambient bubble radius R_0 was measured while the sound field was

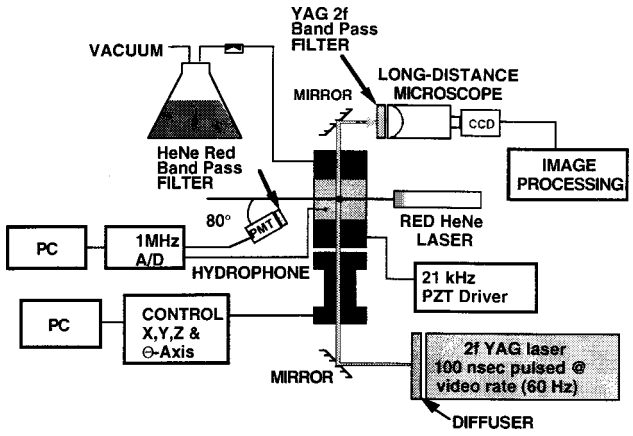

FIG. 1. Apparatus used to study bubble dynamics during single bubble sonoluminescence. The He-Ne laser and the photomultiplier tube were used to monitor the dynamic bubble radius. The imaging apparatus (CCD camera, long-distance microscope, and YAG laser) were used to measure the ambient (R_0) and maximum ($R_{\max}$) bubble sizes. The calibrated hydrophone was used to measure the acoustic pressure.

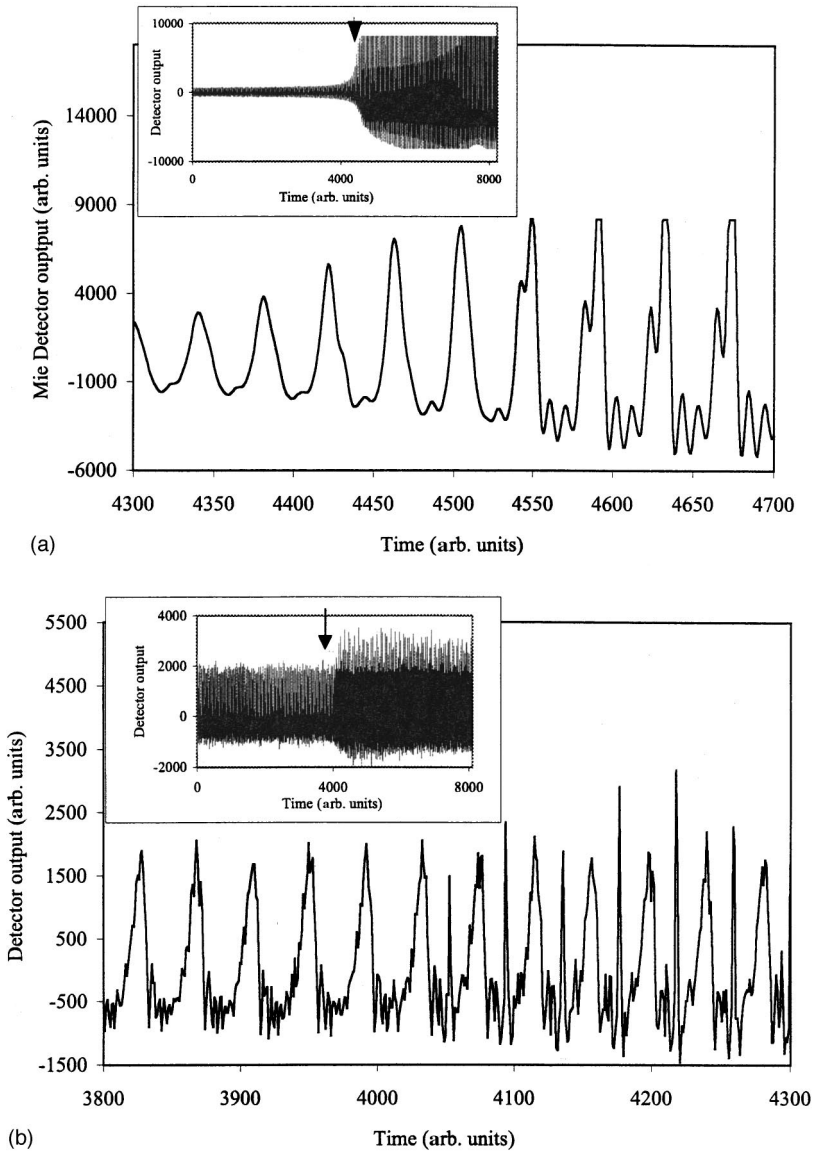

FIG. 2. Mie scattering detector (PMT) output for different bubbles near the transition into shape instabilities. The inset shows the PMT signal before and after the transition, with the arrow marking the approximate location of the data shown in the main plot. (a) $R_0 = 68\ \mu$m, $P_a = 0.19$ bar. The video images indicated an $n = 4$ shape mode. (b) $R_0 = 20\ \mu$m, $P_a = 0.66$ bar. The video images suggested an $n = 3$ shape mode. (c) $R_0 = 6.5\ \mu$m, $P_a = 1.2$ bar. The video images did not have enough resolution to discern a mode. The bubble was *not* emitting light. (d) $R_0 = 7.0\ \mu$m, $P_a = 1.4$ bar. The video images did not have enough resolution to discern a mode. Before the instability occurred, the bubble was emitting light.

momentarily turned off. In cases where the resolution of the bubble image was poor, bubble sizes were calculated using the measured P_a and the maximum bubble size $R_{\max}$ using the Rayleigh-Plesset equation.

In order to measure the threshold for shape instability of the bubbles, two primary observables were monitored: the Mie scattering signal and video images of the bubble (see Fig. 1 for the apparatus). The signal generated by the light scattering at 80° from the forward was subtracted from that generated by forward scattering (pseudoextinction technique, see Ref. [9]), which often resulted in a trigger signal generated when the shape distortions were present. This occurs because the forward scattering is relatively insensitive to deviations from sphericity as compared to the scattering at 80°. The trigger was used to initiate the 1 MHz digital sampling board that recorded both the hydrophone and light scattering signal from the bubble. Shape distortions typically generate large amplitude deviations relative to the spherical Mie scattering signal and are therefore easily detectable. At other times, however, more subtle detection techniques were employed. Video images were recorded using a conventional CCD camera and VCR. The images were then used to identify the particular shape mode by locating the images marked by the analog trigger signal on the audio track of the S-VHS tape. These two methods were successful for bubbles between 15 and 100 μm. For smaller bubbles near the SL regime (at $P_a \geqslant 1$ atm), the video images did not have enough resolution and the Mie scattering spikes due to the shape instability were often too brief (a fraction of a μsec) to trigger the circuit. It was possible, however, to detect the presence of instabilities by monitoring the Mie scattering signal in a fast (100 MHz) oscilloscope. In Figs. 2(a)–2(d) we dis-

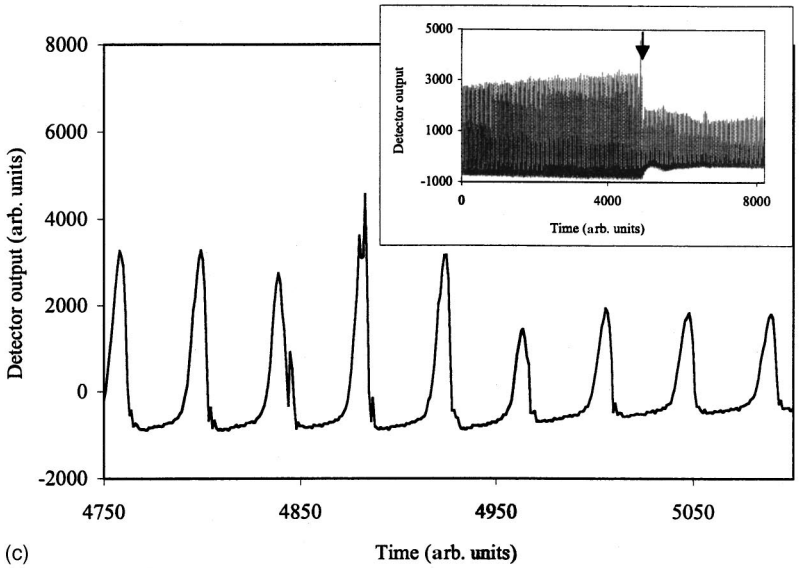

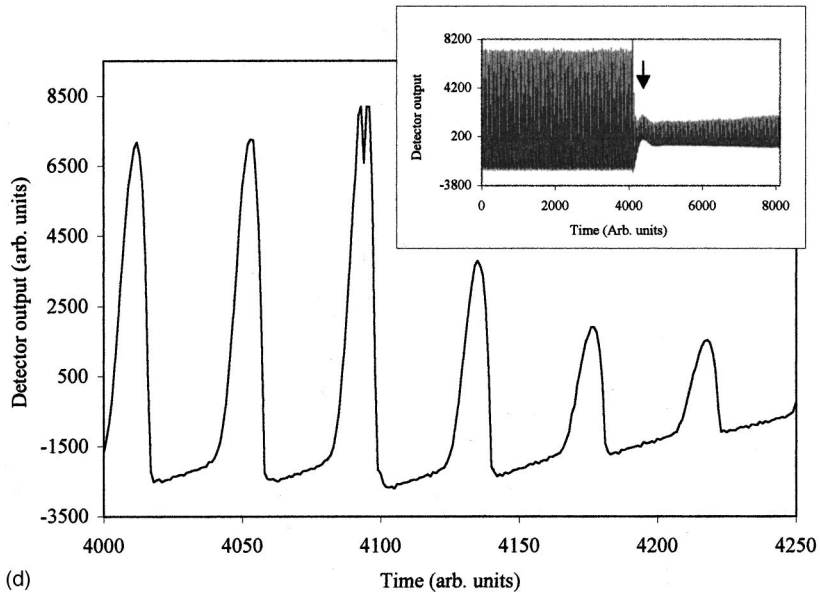

FIG. 2 (*Continued*).

play Mie scattering signals at the onset of a shape mode or shape instability. In these figures we show the variety of symptoms to be encountered when making measurements spanning the range from large bubbles at low driving pressures to small bubbles at high pressures (SBSL).

Figure 2(a) shows the transition to an $n=4$ shape oscillation as the pressure is slightly increased for a relatively large bubble ($R_0=68\,\mu$m) driven at $P_a=0.19$ bar. This type of transition is typical of large bubbles in that the scattered intensity increases by several orders of magnitude, as is demonstrated in this figure by the saturation of the detector. This type of transition tended to be gradual, and the energy coupling can be classified as resulting from resonance. Such resonance is defined by an integer ratio of shape mode frequency to volume mode frequency for forced periodic volume oscillations ([10]; Hilgenfeldt *et al.* in [16]). In Fig. 2(b), a smaller bubble ($R_0=20\,\mu$m) driven at 0.66 bar is shown as an $n=3$ shape instability sets in. Note the spikes caused by the instability. In this size range the energy coupling is still resonant, but the ratio of shape frequency to volume frequency (as determined by observed size and mode) is always $\frac{1}{2}$ within error limits. Note that for these smaller bubbles the relevant volume oscillations are those of the nearly free rebound phase following the main collapse. Furthermore, the frequency of these oscillations is the bubble's natural frequency and therefore the oscillations are only approximately periodic due to nonlinearity.

In Fig. 2(c) a much smaller bubble ($R_0=6.5\,\mu$m) is shown. This bubble is just below the threshold for light emission but is not stable due to insufficient degassing of the water ($C_i/C_0\geqslant 50\%$). Spikes can also be seen here near the bubble collapse. The large decrease in scattering amplitude suggests that the bubble fragmented. In cases like this, the bubble is often observed (via video camera) to break up into two or more smaller fragment bubbles. Many of these fragments are observed to dissolve, but at least one or more coalesce and continue oscillating, growing, and repeating the process. The shape eigenmode (if any) was undetermined due to insufficient video resolution.

In Fig. 2(d), a sonoluminescing bubble ($R_0=7\,\mu$m, $P_a=1.4$ bar) is shown, exhibiting what appears to be a breakup. Even though the gas content was optimum for SL, spikes

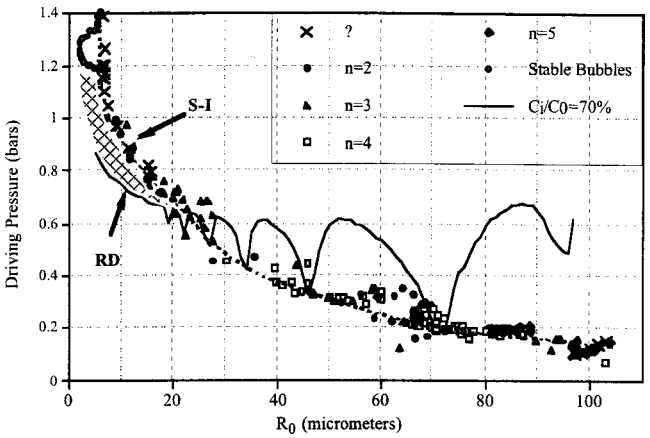

FIG. 3. Peak acoustic pressure amplitude threshold for shape instability (symbols, except open circles) and rectified diffusion (solid line) for 70% gas concentration. ×'s represent unknown shape modes, open circles represent SBSL.

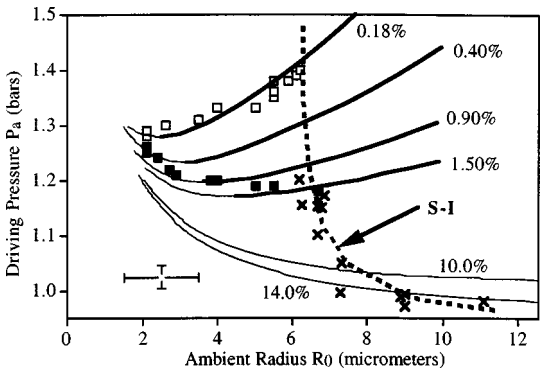

FIG. 4. Measured stable and unstable bubble oscillations represented in the parameter space (P_a, R_0) for a constant preparation value of dissolved air in water, $C_i/C_{0L}=14\%$, and a constant acoustic frequency (20.6 kHz) at 21.7 °C. Solid lines: numerical rectified diffusion equilibrium according to the Eller-Flynn formulation for different values of C_i/C_0. Regions of stable equilibrium are drawn with a thick line. Squares: measured R_0 and P_a data for *stable* bubble oscillations for $C_i/C_{0L}=14\%$. Solid squares are bubbles that do not emit light; open squares represent light-emitting (SBSL) bubbles. The × symbols correspond to the measured shape instability (SI) threshold. The dashed line is an interpolation of the shape threshold data. The approximate error bars for the squares and × symbols are shown in the lower left of the plot.

during and after the rebound (following the initial collapse) were observed as the extinction threshold was approached. These spikes were too short-lived to be recorded by the data acquisition system, but could be easily observed with a 100 MHz (or faster) digital storage oscilloscope. Again, the video resolution was insufficient to determine a shape mode, but fragmentation was observed. The connection between this observation and the sudden extinction of the bubble, which occurs at essentially the same parameters [indeed this particular bubble disappeared a few hundred cycles after the data in Fig. 2(d) were taken] is unclear. It is intriguing that the first indication of instability occurs during a volume expansion, which is normally a stabilizing phase of motion. One potential explanation is that there are two bubbles present, and the split must have occurred at the collapse immediately prior. Matula *et al.* [11] have also observed such scattering signals near the extinction threshold.

GROWTH AND MECHANICAL STABILITY

In Fig. 3, the P_a threshold for SI (labeled ''F'' in [2]) is shown. The symbols (except for the open circles) indicate the shape mode observed immediately after the bubble becomes unstable in an air/water mixture driven at 20.6 kHz. The measurements were obtained at different dissolved gas preparations ranging from near saturation for large bubbles to strongly degassed for the smallest sizes. Resonance conditions, which vary depending on the equilibrium size of the bubble, determined the excited shape mode [10,12]. The maximum bubble radius that can be levitated is ~ 150 μm, which corresponds to the resonance size at 20 kHz. Note that SBSL occurs only in the upper left-hand corner (open circles). This figure serves to illustrate how small the SBSL parameter space is. The solid line corresponds to the RD threshold for 70% dissolved gas (air) concentration (C_i/C_{0L}), where C_i is the concentration in the liquid far from the bubble and C_{0L} is the saturation value at ambient pressure. In general, lower (higher) concentrations will shift the RD curve towards larger (smaller) P_a. We note in passing that in the vicinity of nonlinear bubble response resonances (e.g., the dip in the 70% RD curve near 70 μm in Fig. 3) there are regions where stable diffusive equilibria exist. If these small regions lie below the SI threshold, they will act as attractors for a fixed C_i/C_{0L}. This explains why the SI data appear in several clusters for $R_0 \geqslant 50$ μm.

In the laboratory usually only P_a is controlled, whereas the bubble size is determined by the other experimental parameters. For example, bubbles below the RD threshold will dissolve and those above will grow until they reach the SI threshold. When they reach the SI curve, bubbles will break up and coalesce in a continuous cycle or execute stable nonlinear shape oscillations [13] unless they grow beyond the maximum size for levitation and escape the field. In the case where the SI curve lies below the RD curve, the bubble will dissolve before reaching instability. For this reason, only regions of the P_a, R_0 space where SI is above RD will be available for steady-state experiments. Such a region has been shaded in Fig. 3. At the higher values of P_a ($\geqslant 1$ bar), the breakup and coalescence will occur so quickly that the bubble will remain near the SI curve most of the time. When this is the case, the bubble will start emitting light at around 1.3 bar but in a rather erratic fashion (≈ 1 flash per 10 acoustic cycles) due to its instability. This phenomenon, first reported and explained by Gaitan *et al.* [1], has been more recently termed *unstable SL* [14].

When the value of C_i/C_{0L} is less than 50% and $P_a \approx 1.15$ bar, however, the bubble begins to deviate from the SI curve toward a smaller R_0 (see also Ref. [6]) and becomes stable (Fig. 4, square symbols). The smaller the gas concentration is, the smaller R_0 becomes for a given P_a [see Ref. [2], Figs. 1(a)–1(c)]. As P_a is increased, R_0 first decreases (filled squares, termed *lower branch*) and then increases (open squares, termed *upper branch*) until it reaches the *extinction threshold* where SBSL is no longer observed because the bubble disappears. On the lower branch, the value of C_i/C_0 calculated from the bubble radial motion begins to

decrease as P_a is increased. On the upper branch (see Fig. 2 of [2]), C_i/C_0 reaches a value $\approx$1% of C_i/C_{0L} (the actual gas concentration far from the bubble) and stays constant. At any other point in the observable P_a,R_0 space ($P_a \leqslant 1.15$ bar in shaded region), the value of C_i/C_{0L} appears to equal C_i/C_0.

Figure 4 also shows a family of calculated rectified-diffusion (RD) equilibria for the boundary-layer theory of Eller and Flynn [4]. These curves represent conditions for a net mass flux of zero across the bubble wall averaged over a cycle of the bubble oscillation. They were calculated from the expression

$$\frac{C_i}{C_0}=\left(1+\frac{2\sigma}{R_0P_\infty}\right)\frac{\langle R/R_0\rangle}{\langle (R/R_0)^4\rangle} \tag{1}$$

using a Rayleigh-Plesset model [15] and the measured $R_{\max}$ and P_a; the validity of the Eller-Flynn formulation was experimentally verified in Ref. [2] for $P_a \leqslant 0.9$ and $20\% \leqslant C_i/C_0 \leqslant 50\%$. For larger R_0 these curves have resonant peaks and valleys [16]; however, due to the dominating surface-tension effect [17], they are single-valued at small R_0.

These observations are consistent with Lohse *et al.*'s hypothesis in which the non-noble gases in air (O_2,N_2) begin to react chemically and as a consequence become inactive in the diffusive process. A larger portion of these gases will become inactive as the internal temperatures and pressures increase (due to the larger P_a) until only argon is present inside the bubble. Thus, the effective C_i/C_0 will decrease at first (lower branch) until it reaches a minimum value (upper branch) of 1% of C_i/C_{0L}, which is the same as the proportion of Ar in air.

Furthermore, we propose that even though other processes are affecting the gas diffusion, the standard RD formulation [4] can still be used to explain the growth stability of the bubble if the value of C_i/C_{0L} for the gas concentration far from the bubble is replaced by the smaller value of C_i/C_0 calculated from the observed dynamic bubble radius. This hypothesis is supported by the data in Fig. 4, where the filled squares fall near the points (within the experimental uncertainty) in the RD threshold curve where the slope is positive, thus satisfying condition (iii). A positive slope allows the bubble to be in stable growth equilibrium since the bubble crosses from a growth to a dissolution region as R_0 increases. We attribute the occasional negative slopes for some of the data to experimental error.

Note also that, perhaps coincidentally, light begins to be emitted as the upper branch is reached. At this point, according to Lohse *et al.*'s hypothesis, Ar is expected to fill most of the bubble. Therefore, the inception of light emission might be an indication that Ar is a more efficient gas for the generation of light due to its large heat-capacities ratio. On the other hand, it could be the result of the higher driving pressures P_a, which generate more violent collapses. Several investigators [18] have postulated that at this point the bubble wall velocity has reached the speed of sound in the gas (Mach 1) generating shock waves which are thought to be responsible for the light emission when they converge at the bubble's center.

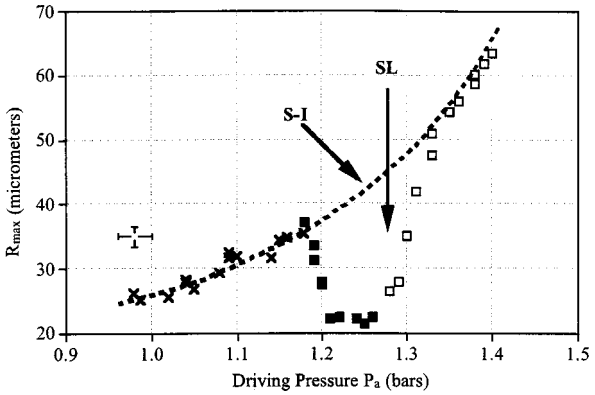

FIG. 5. Measured maximum bubble radius attained during one cycle ($R_{\max}$) as a function of the acoustic pressure for the data in Fig. 3. The dashed line was drawn to represent the path the bubble takes when $C_i/C_0 \geqslant 0.5$ and corresponds to the SI dashed line in Figs. 2 and 3. All experimental parameters and symbols are the same as in Fig. 3.

As noted by others (Refs. [17,19]) for $C_i/C_{0L} < 5\%$, the bubble will stabilize without the need for any mass loss as long as the water can be degassed below this level. This is an important consideration when trying to predict the conditions under which bubbles will stabilize in other liquid-gas mixtures, and is in fact the case in some observations in water/polyatomic-gas mixtures reported by the UCLA group [19].

BUBBLE RESPONSE AND THE THRESHOLD FOR LIGHT EMISSION

Figures 5 and 6 are plots of $R_{\max}$ and $R_{\max}/R_0$, respectively, as functions of P_a for the same data presented in Fig. 4. Both $R_{\max}$ and $R_{\max}/R_0$ grow roughly as power-law functions of P_a along the shape instability threshold, which is indicated by the dashed lines in the figures. The crosses (unstable oscillations) and squares (stable oscillations) depict the data set in water prepared at 14% saturation. The presence of an island of dissolution responsible for the deviation described above causes a resonancelike phenomenon to oc-

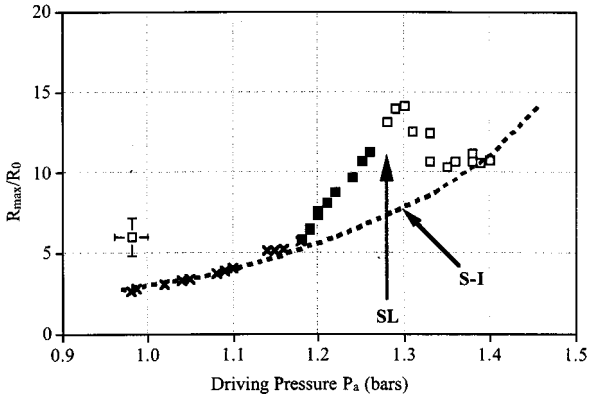

FIG. 6. Measured expansion ratio of the maximum bubble radius attained during one cycle and the ambient radius ($R_{\max}/R_0$) as a function of P_a for $C_i/C_{0L} = 14\%$. The dashed line was drawn to represent the path the bubble takes when $C_i/C_0 \geqslant 0.5$ and corresponds to the SI dashed line in Figs. 2 and 3. All experimental parameters and symbols are the same as in Fig. 3.

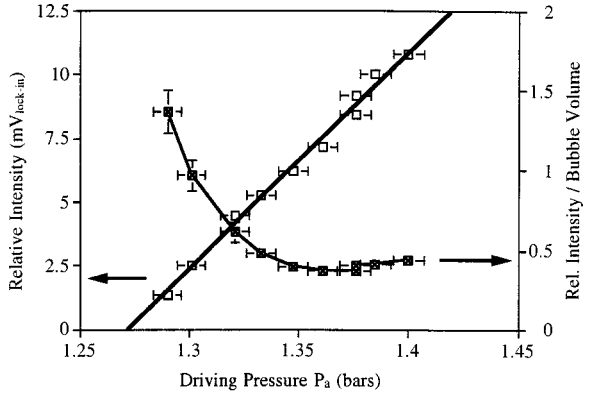

FIG. 7. Number of photons (open squares) and number of photons divided by the bubble volume (crossed squares) emitted during stable SBSL as a function of the driving pressure for $C_i/C_{0L}=14\%$. The number of photons is proportional to the voltage output of the PMT (Hamamatsu H5783-00) which was measured with a lock-in amplifier. The spectral response of the apparatus is ~300–600 nm. All experimental parameters and symbols are the same as in Fig. 3.

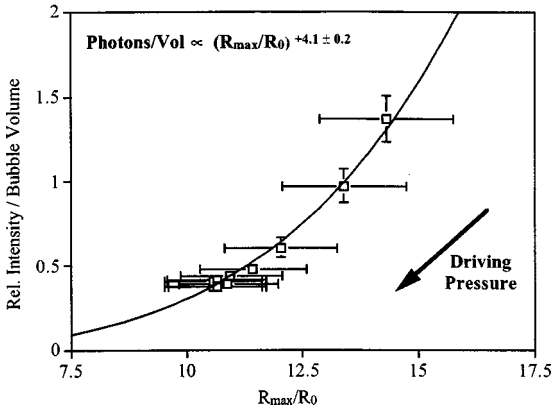

FIG. 8. Number of photons per normalized ambient bubble volume (R_0^3) in arbitrary units as a function of $R_{\max}/R_0$ for $C_i/C_{0L}=14\%$. Note that the acoustic pressure and the ambient size are both *decreasing* from left to right (increasing $R_{\max}/R_0$), as can be inferred from Figs. 3–5. All experimental parameters and symbols are the same as in Fig. 3.

cur. The rapid decrease in ambient radius R_0 seen in the experiment in Fig. 4 causes $R_{\max}$ in Fig. 5 to decrease, reaching a minimum of about 23 μm at the minimum R_0, and then increase as R_0 increases along the upper branch. Note that the light emission threshold, marked by the arrow, occurs on the upper branch and at relatively low values of $R_{\max}$ ($\approx$28 μm), indicating that it is not a unique function of $R_{\max}$. The importance of this observation is that $R_{\max}$ is a measure of the mechanical potential energy stored by the bubble, and hence the velocity of the collapse is roughly proportional to $R_{\max}$. Thus theories based on a collapse velocity threshold will have to take this into account. For this experiment, the light-emission threshold was measured around 1.28 bar.

The expansion ratio $R_{\max}/R_0$ displays a sharp maximum in Fig. 6 of $\approx$15, which appears to lag the minimum value of $R_{\max}$ and R_0. As P_a is further increased from the peak value, $R_{\max}/R_0$ decreases to a value of 10, where it apparently levels off for further pressure increases until the *extinction threshold* [20] at 1.4 bar. We note here that data sets other than those in Figs. 4–6 indicate expansion ratios may reach 20 at the peak (see also Refs. [19,21]).

DEPENDENCE OF LIGHT INTENSITY ON MECHANICAL RESPONSE

Given the highly nonlinear behavior of the bubble wall response shown in Figs. 4–6, it is important to know how the intensity of SL varies with the response. In Fig. 7, the wavelength-averaged light intensity versus acoustic pressure (open squares) is plotted [see Barber *et al.* (1991) in Ref. [1] for a comparison], and the intensity increases linearly with pressure, growing by a factor of 10 from inception at 1.28 bar to extinction at 1.4 bar. Note that R_0 increases and $R_{\max}/R_0$ decreases in the light-emitting regime ($1.28 \leqslant P_a \leqslant 1.4$ bar) as shown in Figs. 4 and 6. Figure 7 also plots the emitted light intensity normalized to the bubble volume R_0^3 (thus roughly a photon per gas molecule efficiency, crossed squares). We see that this normalized intensity decreases as a function of pressure, suggesting that the increase shown in the unnormalized intensity is mostly due to the fact that the bubble volume is increasing (by a factor of 10 from 1.28 to 1.4 bar) and a greater number of molecules is available for light emission. This may quantitatively account for the increase in the total (visible) emitted light intensity as a function of P_a observed in experiments.

Furthermore, the normalized light intensity versus the expansion ratio $R_{\max}/R_0$ is plotted in Fig. 8, and we find that the light output *per gas molecule* is dramatically increased as the expansion is increased. Figure 8 shows a fit to the data with a nearly quartic (4.1 ± 0.2) power-law dependence on the expansion ratio, implying that a hotter, more energetic collapse occurs for smaller bubbles with a greater $R_{\max}/R_0$. The uncertainty in the exponent is due primarily to the uncertainty in the measured P_a.

Since the size of the actual emitting region is unknown and likely depends on R_0, the above interpretation may be somewhat simplistic. For example, it has been argued [22] that the size of the emitting region inside the bubble increases as $R_{\max}/R_0$ increases because the temperature inside the bubble becomes hotter sooner in the collapse phase than at smaller values of the expansion ratio. However, sufficiently sophisticated theories of SBSL which can relate the expansion ratio to the light emission can be directly compared to these measurements. In particular, the onset of SL near the minimum in R_0 but near the maximum in expansion ratio should be a stringent test of those theories.

There are two theoretical treatments that have predicted a sensitive dependence of the light emission on the expansion ratio. Kondic *et al.* [22] solve the gas dynamics allowing for shock waves, and treat emission using both a thermal and a plasma approach to modeling the radiation. Moss *et al.* [22] use essentially the same approach, with a much more detailed equation of state, which includes semiempirical formulas for corrections valid at high temperatures and pressures.

We have attempted to compare the predictions made by Kondic *et al.* [22] (specifically their Table II, p. 4981) with our results, and we find that their predictions of the functional dependence of the number of photons on the expan-

sion ratio depend critically on R_0. For a constant P_a and decreasing R_0 they find that the number of photons per unit volume *decreases* with increasing expansion ratio $R_{\max}/R_0$, which is the opposite of our results in Fig. 8. For increasing P_a and fixed R_0, the number of photons per bubble ambient volume increases more rapidly than our data. Thus, it was impossible to include their numerical results on our graphs for even a qualitative comparison. Figure 3 of Moss *et al.* ([22], 1997) shows that the predicted number of photons per flash doubles as $R_{\max}/R_0$ is increased by only 4%. However, Moss *et al.* use a fixed R_0 so again a direct comparison with our Fig. 8 is not possible.

At a minimum, it is fair to say that the emission is very sensitive to the expansion ratio. It is worth noting here that most experimental spectra [23] have been obtained by ''looking where the light is brightest,'' that is, at the maximum pressure where the total number of photons is greatest. Thus estimates of internal temperatures based on such spectra may well be lower bounds inferred from relatively ''cool'' bubbles.

CONCLUSION

Our measurements indicate that the mechanics of an air bubble in water near the light-emission threshold are not trivial. However, they seem to be well explained by coupling mechanical instabilities, chemical reactions, and gaseous mass diffusion to the nonlinear bubble motion described by the Rayleigh-Plesset equation [7,24]. Our measurements show how the available P_a, R_0 space is bounded by the mechanical instability threshold and the constant C_i/C_{0L} curve. The deviation from the mechanical instability curve can be explained by a gradual decrease in the effective C_i/C_0 seen by the bubble and by requiring a stable rectified diffusion equilibrium to be maintained. This decrease ends when C_i/C_0 reaches a value of 1% of the actual gas concentration far from the bubble (C_i/C_{0L}).

The parametric dependences of the emitted light intensity presented in Figs. 5–8 are unexplained, but represent an effort to clarify the relationship between bubble dynamics and light emission. The power-law dependence of the normalized light intensity on the expansion ratio $R_{\max}/R_0$ is a particularly interesting result.

The difficulties we encountered in attempting to compare our data to available theory lead us to conclude that it is *impossible* to make meaningful comparisons between experiment and theory unless the exact bubble dynamics are taken into account. Based on our measurements, we can extract a minimal set of threshold mechanical criteria for light emission from an air bubble in water at 20 kHz, to be used as bounding conditions for light-emission theories. As long as the emission theory restricts itself to an isolated bubble and a single collapse, issues surrounding the dissolved gas content of the water can perhaps be ignored. The conservative domain of radii for bubbles in pure water is $2 \leqslant R_0 \leqslant 7\ \mu$m. The range of acoustic pressures is $1.3 \leqslant P_a \leqslant 1.4$ bar at 1 bar ambient pressure. The range of expansion ratios corresponding to the above domain of R_0 is $10 \leqslant R_{\max}/R_0 \leqslant 15$. As we have shown, however, these parameters are dependent on each other via the mass transfer across the bubble.

ACKNOWLEDGMENTS

This work was supported by NASA. We thank M. Brenner, S. Hilgenfeldt, J. Holzfuss, D. Lohse, W. Moss, R. Roy, and E. Trinh for stimulating discussions. We thank E. Trinh for loaned equipment.

[1] D. F. Gaitan and L. A. Crum, in *Proceedings of the 12th International Symposium on Nonlinear Acoustics, Austin, TX, 1990*, M. F. Hamilton and D. T. Blackstock (Elsevier, New York, 1990), p. 459; D. F. Gaitan *et al.*, J. Acoust. Soc. Am. **91**, 3166 (1992); B. P. Barber and S. J. Putterman, Nature (London) **352**, 318 (1991).

[2] R. G. Holt and D. F. Gaitan, Phys. Rev. Lett. **77**, 3791 (1996).

[3] G. I. Taylor, Proc. R. Soc. London, Ser. A **201**, 192 (1950); M. S. Plesset, J. Appl. Phys. **25**, 96 (1954); G. Birkhoff, Q. Appl. Mech. **13**, 451 (1956); M. Faraday, Philos. Trans. R. Soc. London **121**, 299 (1831); H. W. Strube, Acustica **25**, 289 (1971); J. Miles, J. Fluid Mech. **248**, 671 (1993); A. I. Eller and L. A. Crum, J. Acoust. Soc. Am. **47**, 762 (1970).

[4] A. Eller and H. G. Flynn, J. Acoust. Soc. Am. **37**, 493 (1965); R. K. Gould, *ibid.* **56**, 1740 (1974); C. C. Church, *ibid.* **83**, 2210 (1988); M. M. Fyrillas and A. J. Szeri, J. Fluid Mech. **277**, 381 (1994).

[5] We have changed terminology here from the more historical *equilibrium* to *ambient* radius to avoid confusion. In this paper the term equilibrium is associated with processes that are in dynamic (rather than static) equilibrium.

[6] The observation that bubbles in this regime apparently violated the restrictions of convective diffusion for air dissolved in water was made by R. Löfstedt *et al.*, Phys. Rev. E **51**, 4400 (1995).

[7] D. Lohse *et al.*, Phys. Rev. Lett. **78**, 1359 (1997); D. Lohse and S. Hilgenfeldt, J. Chem. Phys. **107**, 6986 (1997).

[8] G. M. Hansen, Appl. Opt. **24**, 3214 (1985); R. G. Holt and L. A. Crum, *ibid.* **29**, 4182 (1990).

[9] J. S. Stroud and P. L. Marston, J. Acoust. Soc. Am. **94**, 2788 (1993).

[10] R. Glynn Holt and D. Felipe Gaitan, *The Onset of Resonance-Controlled Instability in Spherical Bubble Oscillations, Proceedings of the 3rd Microgravity Fluid Physics Conference, Cleveland, 1996*, NASA CP 3338 (NASA, Cleveland, 1996), p. 591.

[11] T. J. Matula and L. A. Crum, *Proceedings of the 16th International Congress on Acoustics/135th Meeting of the Acoustical Society of America, Seattle, Washington*, edited by P. Kuhl and L. Crum (ASA, New York, 1998), p. 2585.

[12] R. G. Holt and D. F. Gaitan (unpublished).

[13] R. G. Holt, J. Holzfuss, A. Judt, A. Phillip, and S. Horsburgh, in *Proceedings of the 12th International Symposium on Nonlinear Acoustics, Austin, Texas*, edited by M. F. Hamilton and

D. T. Blackstock (Elsevier, New York, 1990), p. 497.
[14] B. P. Barber *et al.*, Phys. Rev. Lett. **72**, 1380 (1994); K. Weninger *et al.*, J. Phys. Chem. **99**, 14195 (1995).
[15] A. Prosperetti *et al.*, J. Acoust. Soc. Am. **83**, 502 (1986).
[16] D. F. Gaitan, dissertation, University of Mississippi, 1990; M. Brenner *et al.*, Phys. Rev. Lett. **76**, 1158 (1996); S. Hilgenfeldt *et al.*, Phys. Fluids **8**, 2808 (1996).
[17] I. Akhatov *et al.*, Phys. Rev. Lett. **78**, 227 (1997); S. Hilgenfeldt *et al.*, JFM in press.
[18] P. Jarman, J. Acoust. Soc. Am. **32**, 1459 (1960); B. P. Barber *et al.*, Phys. Rev. Lett. **72**, 1380 (1994); Hilgenfeldt *et al.*, in Ref. [15].
[19] B. P. Barber *et al.*, Phys. Rev. Lett. **74**, 5276 (1995); R. Löfstedt *et al.*, Phys. Fluids A **5**, 2911 (1993).
[20] S. M. Cordry, Ph.D. thesis, University of Mississippi (1995); S. M. Cordry and L. A. Crum, J. Acoust. Soc. Am. **97**, 3375 (1995); T. J. Matula *et al.*, *ibid.* **100**, 2717 (1996).
[21] R. Hiller *et al.*, Science **266**, 248 (1994).
[22] W. C. Moss *et al.*, Phys. Lett. A **211**, 69 (1996); W. C. Moss *et al.*, Phys. Fluids **6**, 2979 (1994); L. Kondic, J. I. Gersten, and C. Yuan, Phys. Rev. E **52**, 4976 (1995); W. C. Moss *et al.*, Science **276**, 1398 (1997).
[23] R. Hiller *et al.*, Phys. Rev. Lett. **69**, 1182 (1992); T. J. Matula *et al.*, *ibid.* **75**, 2602 (1995); D. Felipe Gaitan *et al.*, Phys. Rev. E **54**, 525 (1996).
[24] L. Kondic and J. I. Gersten, J. Acoust. Soc. Am. (to be published).